Micron 120 (2019) 74–79

Contents lists available at ScienceDirect

Micron

journal homepage: www.elsevier.com/locate/micron

Electron beam damage of epoxy resin films studied by scanning transmission X-ray spectromicroscopy

Weiwei Zhang[a], Lis G. de A. Melo[b], Adam P. Hitchcock[b], Nabil Bassim[a,*]

[a] Department of Materials Science and Engineering, McMaster University, Hamilton, ON, Canada
[b] Department of Chemistry & Chemical Biology, McMaster University, Hamilton, ON, Canada

ARTICLE INFO

Keywords:
Electron beam damage
Scanning transmission X-ray microscopy
Carbon deposition
Epoxy resin film

ABSTRACT

Focused ion beam coupled with scanning electron microscopy (FIB-SEM) is a popular technique for advanced electron microscopy with applications such as, high-precision site-specific lamella sample preparation for transmission electron microscopy (TEM) and slice-and-view FIB 3-dimensional tomography. Damage caused by the electron imaging component of FIB-SEM may be compounded with damage from the ions during the ion milling process. There are known strategies for mitigating damage from ions and electrons (cryo-SEM, dose-control, voltage control), but the electron damage on common embedding resins for EM has not been explored in detail beyond their resistance to shape-change. The relationship between beam parameters and damage mechanisms remains unclear. Since we are relying on the physical, chemical and thermal stability of embedded samples during ion-beam milling, it is important to distinguish electron beam damage from ion beam damage. Scanning transmission X-ray microscopy (STXM) has been used for analyzing the electron beam radiation damage on polymer films by characterizing the chemical bonding changes. In this paper, we focus on the effect of beam voltage and electron dose on electron beam damage to epoxy resin thin films. Irradiated areas on polymer thin films were characterized by near edge X-ray absorption fine structure (NEXAFS) in STXM. We found that, even when using low current and voltage, the electron beam can still cause noticeable chemical changes within the polymer film. The degree of electron beam damage depends not only on the beam energy, but also on the amount of inelastic scattering occurring within the material, as determined by the sample thickness.

1. Introduction

Coupled with scanning electron microscopy (SEM), focused ion beam (FIB) microscopy is used extensively for high precision site-specific lamella sample preparation for transmission electron microscopy (TEM), 2D piezoelectric materials preparation, nano-milling, and 3D FIB tomography (Bassim et al., 2014; Burnett et al., 2016; Giannuzzi and Stevie, 1999; Li et al., 2018a, b). However, for soft materials, their higher sensitivity to the ion/electron irradiation and lower thermal conductivity (Egerton et al., 2004, 2006) pose challenges. To achieve high-quality FIB prepared samples and milling process for 3D tomography, a further understanding of the damage mechanisms involved in the FIB-SEM system needs to be explored. Previous research found that the chemical damage in soft materials is mainly caused by the electron beam (Bassim et al., 2012). Compared with the curtaining artifacts and heating damage, the chemical changes induced by the electron irradiation during the SEM component of FIB/SEM are usually neglected when considering the milling process, but its effect may not be negligible (Bassim et al., 2012).

Researchers have studied electron beam (e-beam) damage in perovskite materials, nanomaterials, and polymers and have had some success in understanding the damage features in these materials and the underlying mechanisms (Lehnert et al., 2017; Rothmann et al., 2018; Wang et al., 2009a; Xu et al., 2011). Due to the wide variability of soft materials, few solid conclusions have been drawn to explain the damage mechanisms prescriptively enough for practical applications in the FIB-SEM.

The material chosen for this study was EMbed 812 epoxy resin, a popular polymer for embedding biological samples for TEM study and FIB-SEM 3D tomography (Tapia et al., 2012). Bubbling and chemical degradation which can come from the electron beam damage (Koval et al., 2003; Scott, 2011) often limits the high-quality sample preparation or milling of biomaterials. Little research has been carried out on the chemical changes due to the electron beam irradiation of epoxy resin embedding polymers (Longieras et al., 2007).

In this paper, we studied the effects of beam voltage and dose on

* Corresponding author.
E-mail address: bassimn@mcmaster.ca (N. Bassim).

https://doi.org/10.1016/j.micron.2019.02.003
Received 3 December 2018; Received in revised form 5 February 2019; Accepted 6 February 2019
Available online 07 February 2019
0968-4328/

low-energy electron induced damage to 100 nm thick epoxy resin thin films. The damaged areas were created in a 3 × 3 scanning pattern on the resin thin film by a scanning electron microscope. The irradiated areas were later characterized with near-edge X-ray absorption fine structure (NEXAFS) in a scanning transmission X-ray microscope (STXM) (Hitchcock, 2012) at 10ID1 beamline at the Canadian Light Source (CLS). We found that, even at low beam current, the electron beam can still cause chemical alteration and carbon contamination on the resin thin film. We also found that, at the same electron dose, the degree of electron beam damage depends on the amount of inelastic scattering occurring within the material, which is determined in part by the thickness of thin film polymer samples. In this situation the beam voltage used for FIB-SEM applications such as TEM sample preparation and serial sectioning becomes an important parameter. Carbon contamination, as a dynamic result of the mass loss and deposition process, was observed to be most severe in the case of the 2 kV imaging condition used in this study.

2. Materials and methods

2.1. Preparation of polymer films

The EMbed812 epoxy resin (Electron Microscopy Science) was synthesized following the manufacturer protocol: 20 mL EMbed812, 9 mL Dodecenylsuccinic anhydride (DDSA), 12 mL N-methylolacrylamide (NMA), and 0.72 mL 2,4,6-Tris (dimethylaminomethyl) phenol (DMP-30) was mixed and cured at 60° C for 24 h. The cured resin was then sectioned to about 100 nm films by a Leica ultramicrotome (model Leica Ultracut UCT). The sectioned resin film was then placed on a 200 mesh Cu grid which had been coated previously with 30 nm formvar carbon and 5 nm sputter-coated gold. The formvar supports the resin thin film and provides film-grid adhesion, while the gold layer is used to minimize charging during SEM exposure.

2.2. Electron irradiation patterning

The electron beam patterning irradiation was done using a ThermoFischer-FEI Magellan 400 SEM. Before the irradiation patterning, the microscope chamber was cleaned by a plasma cleaner for 20 min resulting in a vacuum of $5 \times 10^{-4} Pa$. The beam current was fixed to be 50 pA through the whole study to minimize both carbon contamination and charging. The voltage of the electron beam was varied from 1 kV to 5 kV to cover commonly-used parameters for imaging soft materials (Joy and Joy, 1995, 1998). Each exposed area was approximately $3\mu m \times 2\mu m$. As mentioned by Egerton, the typical critical dose for organic materials in TEM application is 0.01 C/cm^2, (Egerton et al., 2012). In this experiment, we did not install a Faraday cup for measuring the exact beam current, so the exposure (which is proportional to dose for thin samples) was calculated using

$$\text{Exposure} = \frac{\text{Beam current} \times \text{Exposure time}}{\text{Scanning area}} \quad (1)$$

The beam current and the scanning area were fixed while the exposure time was varied to get the desired electron dose. A 3 × 3 scanning pattern was used and the dose parameters are reported in Table 1. Python scripts were used to control the exposure time and create the pattern automatically to reduce the effect of unwanted electron irradiation due to manual operation. For clarification, the term 'dose' commonly used in electron-microscopy studies usually refers to the electron exposure (fluence, units of C/cm^2), rather than true radiation dose (absorbed energy per mass, in units of $J/kg = Gray$) used for quantifying radiation damage in studies with other irradiation methods (Du and Jacobsen, 2018; Egerton et al., 2004). For thin samples this is a reasonable approximation since the energy deposited by inelastic scattering is only a small portion of the total e-beam energy (Jiang and Spence, 2012). In this study, the irradiation process was strictly controlled by the computer program with fixed beam current and scanning area. The computer-controlled exposure time was varied to achieve the desired doses.

Table 1
Beam parameters used for the scanning pattern.

Voltage	Dose & Exposure Time		
	0.1 C/cm^2 (200 secs)	0.01 C/cm^2 (20 secs)	0.001 C/cm^2 (2 secs)
5 kV	Area 1	Area 2	Area 3
2 kV	Area 4	Area 5	Area 6
1 kV	Area 7	Area 8	Area 9

2.3. Materials characterization

The irradiated resin film was characterized by using near-edge fine-structure absorption spectroscopy (NEXAFS) measured in the ambient (temperature) scanning transmission X-ray microscope (STXM) at the 10ID-1 beamline at the Canadian Light Source (CLS). A defocused beam size of 250 nm and a step (pixel) size of 250 nm were used to avoid any X-ray damage. Imaging at 288.3 eV, an energy very sensitive to radiation damage, after STXM acquisition did not show any damage (see supplementary information Fig. S-1). The optical density (OD) at each photon energy was calculated from the transmitted intensity, I, and the incident intensity, I_0, using the Lambert-Beer law: $OD = -\ln\left(\frac{I}{I_0}\right)$ OD= $-\ln(\frac{I}{I_0})$ (Stöhr, 2013). Peaks in the absorption spectra are related to excitation of inner-shell electrons to unoccupied molecular orbitals. C 1s and O 1s image sequences (also called stacks) (Jacobsen et al., 2000) were acquired.

2.4. Monte Carlo simulation

The electron trajectory was simulated using a Monte Carlo simulation package, named monte CArlo SImulation of electroN trajectory in sOlids (CASINO v2.5.0) (Drouin, 2011).

Since the chemical formula of the EMbed 812 resin is unknown and proprietary, we chose 100 nm PMMA thin films as the simulated material model due to the similarity of the STXM spectra of Embed812 and PMMA (see supplementary information Fig. S-2). 1, 2 and 5 kV beam voltage cases were simulated, with the beam size of 10 nm set as default. The remaining parameters were set to default values.

3. Results

An optical image of the electron beam 9-pad irradiated pattern is shown in Fig. 1a. An image sequence, consisting of images at 93 photon energies from 278 to 320 eV was measured, aligned and converted to optical density. Fig. 1b are C 1s spectra extracted from the undamaged area between the pads and from the most heavily damaged pad (pad #4). The aligned, optical density image sequence was fit to these two C 1s spectra (Fig. 1b) to generate component maps of the undamaged and damaged resin. Fig. 1c is a color-coded composite with the undamaged map from the C 1s fit in green and the damaged map in red. Fig. 1d presents the O 1s spectra extracted from the undamaged region and from the most heavily damaged pad (pad #4). Fig. 1e is a color-coded composite with the undamaged map in green and the damaged map from the O 1s fit in red. The color composites show that the largest extent of damage occurred for a beam energy of 2 kV and the longest exposure time used (200 s). This indicates a relationship between the extent of damage and the physical appearance of the irradiated areas under the optical microscope and STXM. Based on the spectra in Fig. 1 (b) (d), one can also see that the chemical bonding changes dramatically between the undamaged part and the severely irradiated part of the resin film. From the pixel intensity histogram of the non-irradiated

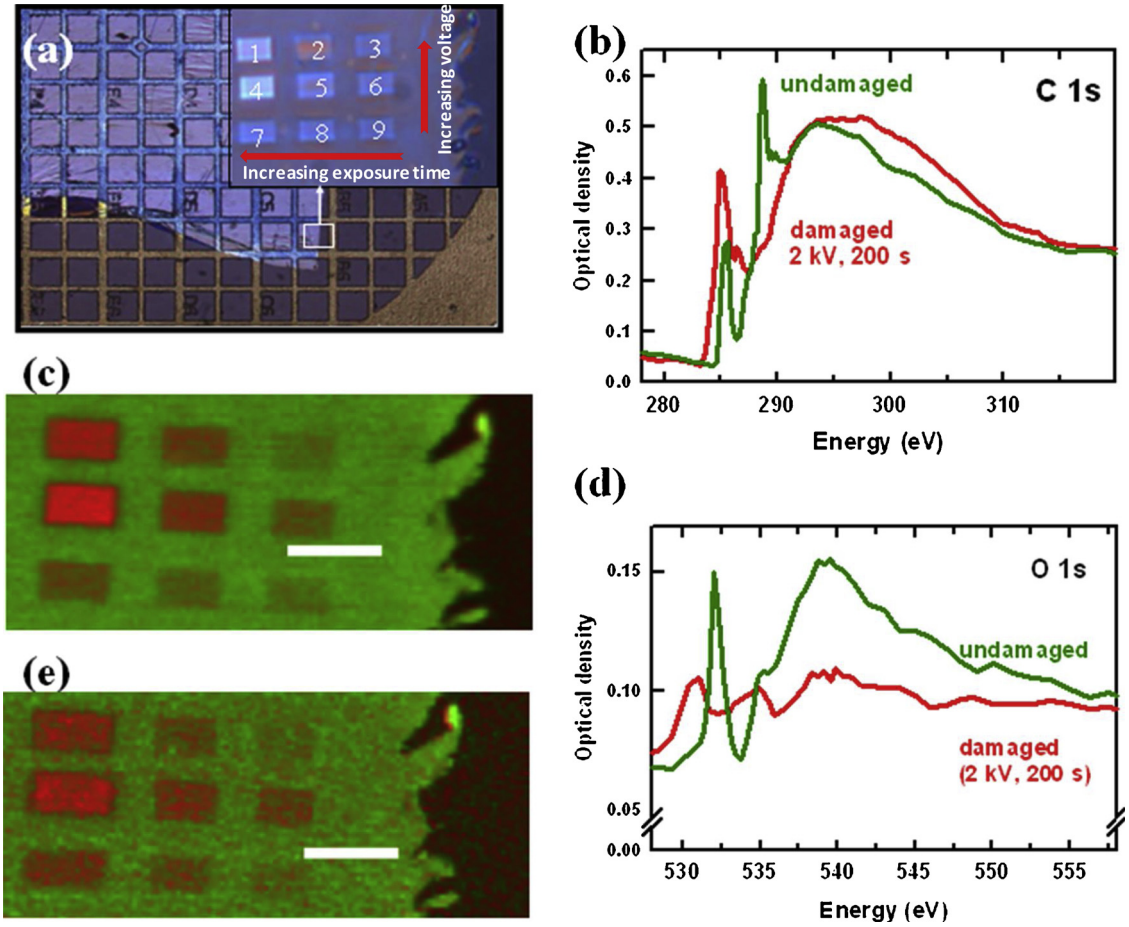

Fig. 1. (a) Reflection mode optical image of the 100 nm resin thin film on the TEM grid. A magnified image of the 9-pad irradiated areas outlined by the white box is inset in the upper-right corner. (b) C 1s spectra of undamaged and damaged (pad 4) resin, taken from a 93 energy stack measured by STXM using a defocused spot to minimize X-ray damage. (c) Color coded composite of the undamaged (green) and damaged (red) component maps obtained by fitting the C 1s stack to the spectra in Fig. 1b. (d) O 1s spectra of undamaged and damaged (pad 4) resin, taken from a 54 energy stacks measured by STXM using a defocused spot. (e) Color coded composite of the undamaged (green) and damaged (red) component maps obtained by fitting the O 1s stack to the spectra in Fig. 1d. The scale bars in Fig. 1c, 1e are 5 μm (For interpretation of the references to colour in this figure legend, the reader is referred to the web version of this article.).

area (supplementary information Fig. S-1), the resin film appears to be uniform. Given that the sample is uniform, it appears that the 2 kV electron beam generates more damage to the resin film than the 1 and 5 kV electron beams, for the same exposure time.

The C 1s NEXAFS spectra of the resin film areas damaged by the 1, 2, and 5 kV electron beam are shown in Fig. 2. The STXM spectrum of the non-irradiated area is also plotted. There are three main features of the non-damaged resin spectrum: the C 1s (C—H) → $1\pi^*_{C=C}$ transition at 285.3 eV, the C 1s (C═O) → $1\pi^*_{C=O}$ transition at 288.4 eV, and a broad continuum peak centered around 293.2 eV due to C 1s (C—H) → $1\sigma^*_{C\text{-}C}$ transitions (Urquhart and Ade, 2002).

3.1. Chemical analysis of full C 1s spectra

With longer exposure time a new peak arises at 286.6 eV which is related to the formation of $C-O$ bonds (see Fig. 2). The intensity of

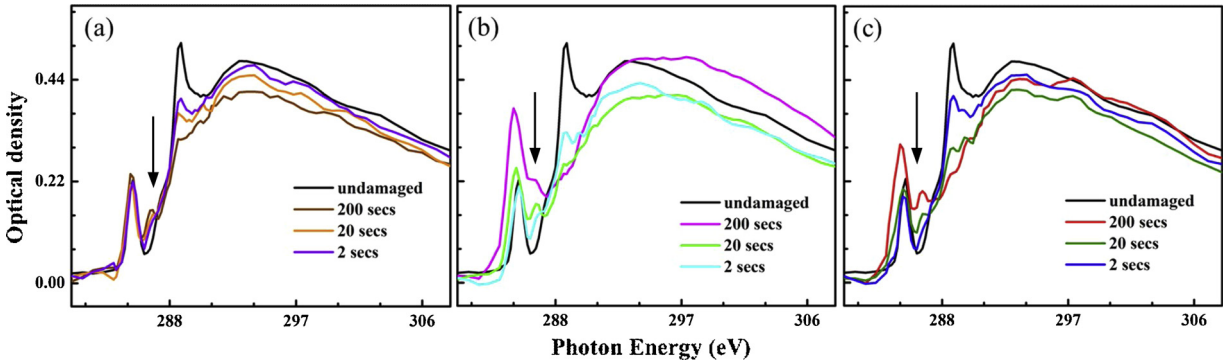

Fig. 2. Comparison of the C 1s spectra of the resin thin film irradiated areas by an electron beam at 2, 20 and 200 s using a beam voltage of (a) 1 kV, (b) 2 kV, and (c) 5 kV. The STXM spectrum of undamaged sample is plotted as black line in each graph as the reference. The arrow in each figure shows the position of the newly created C 1s → $\sigma^*_{C\text{-}O}$ damage peak at 286.6 eV.

this peak increases with longer exposure times and thus is due to electron irradiation damage to the resin thin film. Similarly, the intensity of the 288.4 eV peak (most likely a C 1s → $\pi^*_{O-C=O}$ transition) decreases with increasing exposure time in all cases. The height and shape of the broad peak at 293 eV changes with the exposure time as well as with the electron beam voltage. The peak height decreases with the exposure time when the applied beam voltage is 1 kV, which is similar to the trend of the intensity of the 288.4 eV peak. In the case of 2 kV beam voltage, a 20 s exposure time led to the lowest intensity of the 293 eV peak while the 200 s irradiation resulted in the highest intensity. The shape of the 293.2 eV also becomes broader after 20 s electron beam irradiation as shown in Fig. 2 (b). For 5 kV electron beam irradiation, the 293 eV peak is the weakest for 20 s exposure. The height of the 293 eV peaks in the spectra of the 2 and 200 s irradiated pads are similar but have different peak widths. The increase of the 285.3 eV peak and the broadening of the 293 eV peak may be signatures of deposited amorphous carbon (Leontowich and Hitchcock, 2012). Based on the changes of the peak height and shape of the 9 irradiated areas, the area with 2 kV electron beam irradiation for 20 s is identified as the area with the most severe carbon contamination caused by the electron beam deposition.

3.2. Effect of beam voltage and exposure time on the radiation damage

To study the chemical changes mainly from the radiation, we select the areas with minimal carbon contamination for comparison, region 3,6,9 for studying the influence of beam voltage and region 7, 8, 9 for studying the effect of exposure time. Fig. 3(a, b) shows the C 1s spectra of selected irradiated areas, for the purpose of studying the effect of beam voltage and exposure time on the damage induced by the radiation. Fig. 3(a) shows the spectra of the irradiated areas under 1 kV beam voltage irradiation with varied exposure time, where the carbon contamination is minimal. The extent of radiation damage increases with the exposure time as indicated by the increase in the intensity of the 286.6 eV peak and the diminishing of the 288.4 eV peak. The decrease of the 288.4 eV peak with exposure time indicates that the electron beam damage breaks $C = O$ bonds. Similar observations were found in previous STXM studies of photon irradiated PMMA films (Leontowich et al., 2012; Wang et al., 2009b). Similarly, in Fig. 3(b), the 2 kV electron beam resulted in the most severe radiation damage to the 100 nm resin thin film. The carbon contamination was minimized with 2 s exposure time.

Fig. 3(c, d) show the corresponding O 1s spectra for the same areas selected in Fig. 3 (a, b). The sharp peak at 532 eV in the spectrum of the non-irradiated area is due to O 1s → $\pi^*_{C=O}$ transitions. With longer exposure time, the 532 eV peak decreases and shifts to lower energy, which are signatures of radiation damage in the O 1s spectrum. The decrease in intensity of the 538.5 eV peak indicates that the resin film lost oxygen with longer exposure time. For 2 s irradiation, the 2 kV electron beam resulted in the most significant peak shift and peak drop, indicating the most severe damage, consistent with the result of Fig. 3 (b).

3.3. Monte Carlo simulation by CASINO

Due to the unknown chemical composition of this commercial polymer, we selected PMMA as the material to simulate the electron trajectory and the distribution of inelastic electron scattering. The

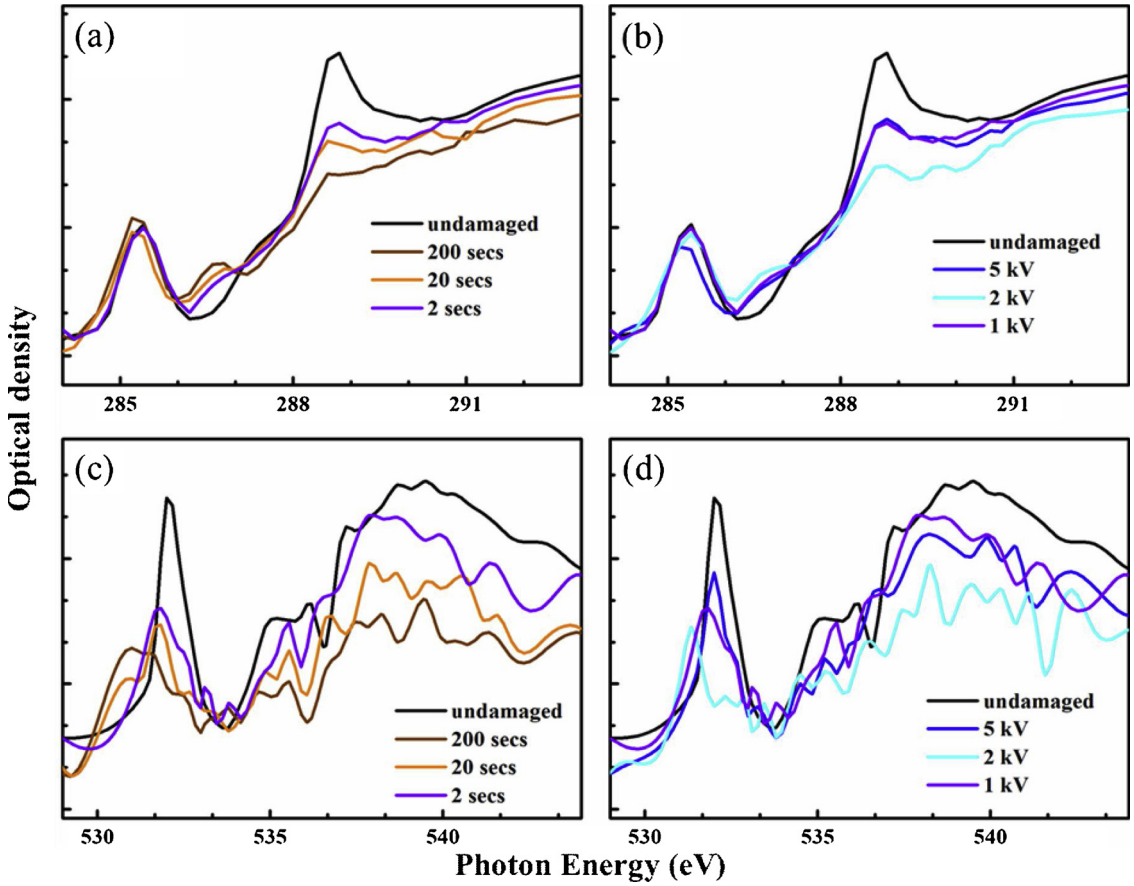

Fig. 3. C 1s and O 1s spectra of radiation damaged resin thin film. (a) C 1s spectra for 1 kV electron beam irradiation for 2 s, 20 s and 200 s. (b) C 1s spectra for 2 s irradiation with voltages of 5 kV, 2 kV and 1 kV. (c) O 1s spectra for 1 kV electron beam irradiation for 2 s, 20 s and 200 s exposure. (d) O 1s spectra for 2 s irradiation with voltages of 5 kV, 2 kV and 1 kV.

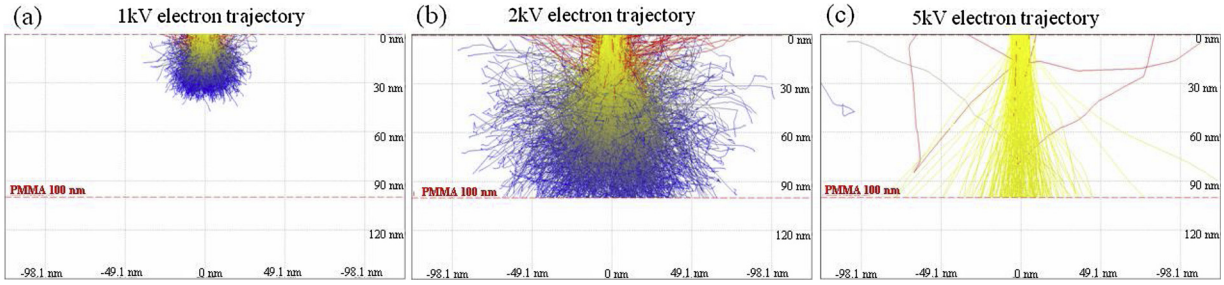

Fig. 4. CASINO Monte Carlo simulation of electron trajectory in 100 nm PMMA thin film with beam voltages of (a) 1 kV, (b) 2 kV, and (c) 5 kV. The red lines refer to the simulated tracks of backscattered electrons that exit the sample. The yellow to blue transition indicates the electron energy decreasing from the incident energy to lowest allowed energy, 0.0001 keV, in each simulated track (For interpretation of the references to colour in this figure legend, the reader is referred to the web version of this article.).

simulated electron trajectory results for the 1, 2 and 5 kV beam voltages are shown in Fig. 4. For a 100 nm polymer thin film, the depth of the interaction volume for a 1 kV electron beam is about 40 nm, and the inelastic scattering region is confined to a relatively shallow volume of the thin film. The depth of the interaction volume for a 2 kV electron beam is around 100 nm, similar to the thin film thickness, and the inelastic scattering is distributed across a quite large width of the thin film. The 5 kV electron beam requires a larger interaction volume than provided by the resin film so that most electrons pass through the sample and the probability of inelastic scattering within the film is much lower. The simulation graphically illustrates why the 2 keV beam energy exhibits the highest extent of radiation damage.

4. Discussion

There are two main types of electron beam damage categorized by different electron-matter interactions: elastic scattering due to electron-nucleus interaction (knock-on) and inelastic scattering due to electron-electron interaction (radiolysis) (Egerton et al., 2004). Soft materials, like organic specimens and biomaterials, are very sensitive to inelastic scattering of the electrons and are often degraded by the radiolysis damage (Egerton et al., 2004, 2006). Beam heating may also be a problem for thin films. For example, a polymer thin film may encounter a few hundred degrees temperature rise if it is under stationary electron beam irradiation (Egerton et al., 2004). However, the heating effect can be negligible under small beam current conditions for most beam diameters in a scanning mode due to the small dwell time (Egerton et al., 2004). Therefore, the electron beam damage mechanisms discussed in the following are limited to e-beam induced mass loss (knock-on), structural damage and mass loss (radiolysis), and e-beam induced deposition (i.e. carbon contamination).

Before we did the irradiation patterning process, we confirmed that the damage observed by STXM came from the intentional electron beam exposure rather than a mixture of intentional patterned damage and background irradiation caused by the navigation process for locating the desired area. To do this we used STXM to measure the spectrum of a pristine resin thin film which never went into the SEM chamber. The STXM spectrum of the pristine resin film and the spectra of regions with no intentional irradiation on the damaged film are essentially the same (see Supporting Information, Fig. S-3). The spectral shapes are identical; there is only a small change of the absolute OD which is due to slightly different thicknesses of the two films. Therefore, we can say that chemical change induced by navigation imaging and residence in the SEM chamber is negligible.

4.1. Carbon contamination

Carbon contamination due to electron beam induced carbon deposition is a common problem in SEMs and may be the result of competition between induced mass loss and gain processes (Egerton et al., 2004). As we discussed in section 3.1 for the case of 1 kV beam irradiation, the C 1s continuum peak height decreases with longer exposure time mainly due to net mass loss. The effect of carbon contamination is minimal. When the beam voltage was 2 or 5 kV, the amount of carbon first decreases with longer exposure time due to mass loss, which we attribute to the electron beam-induced mass loss and radiolysis, and then increases due to beam-induced carbon deposition. In addition to the increase in the C 1s → σ* signal at 293 eV, another spectral signal of cracked carbon is growth of the C 1s → $\pi^*_{C=C}$ peak at 285 eV. This is very significant, especially in the 2 kV electron beam irradiated pads. At relatively low voltages, the deposition rate may grow faster than the mass loss rate with increasing voltage. When a 2 kV beam voltage is used the deposition process dominates, resulting in more deposited amorphous carbon. Under 5 kV electron beam irradiation, the mass loss process catches up with the deposition process, so the relative carbon content of the 5 kV irradiated areas appear to be similar with each other. The change of relative carbon content with different exposure time calculated from the STXM spectrum image can be found in the Supporting information Fig. S-4(a) which confirms that the 2 kV e-beam did lead to more severe mass loss as well as more carbon deposition. One may also notice that a new peak at 286.6 eV appears in the spectra of all damaged areas (Fig. 2), which is a feature specific to radiolysis damage of the resin film.

4.2. Beam voltage and exposure time effect and Monte Carlo simulation

Based on the previous section, we know that higher beam voltage and longer exposure time can lead to significant deposition and mass loss processes. To characterize the chemical changes from radiolysis, we used 1 kV and 2 s exposure time as the baseline for minimum carbon contamination. Under 1 kV beam irradiation, more damage will be introduced with longer exposure time, appearing as a lowered carbon content, as shown in Fig. S-4. The chemical bonding environment also changes with increased exposure time and appears as a drop of the 288.4 eV peak and a rise of the 286.6 eV peak. However, the amount of inelastic scattering events, which is the main cause of the chemical structure change, is not related linearly to the beam voltage, due to the strong change in range with beam voltage for the kV studied. In fact, in the case of a 100 nm resin film, 2 kV beam voltage leads to more radiolysis damage than 5 kV. This can be explained with the assistance of the results of the beam energy dependence of the electron trajectories in a 100 nm PMMA thin film which was simulated by the CASINO Monte Carlo simulation package. From the simulated results, at 2 kV beam voltage, the interaction volume is very similar to the thin film thickness, with a distribution of inelastic scattering very uniformly spread across the whole width of the film. In contrast, many of the 5 kV electrons pass completely through the thin film without inelastic scattering so that the total number of inelastic scattering events is much smaller than at 2 kV. For the 1 kV case, the interaction volume is quite small compared to the whole resin thin film thickness, confining the

damage zone only to the top surface of the film and resulting in less damage. Fig. S-4(b) gives a more direct view on the changes in the amount of C═O bonds as a function of exposure time and beam voltage. The extent of chemical change induced by the electron beam irradiation depends on how efficiently the inelastic scattering is distributed across the thin film. Comparison of the exposure and beam voltage effects for all of the spectra are presented in Figs. S-5 and S-6).

For FIB-SEM serial sectioning tomography with a plasma FIB, the single slice thickness is usually around 100 nm, similar to the film thickness in this study. For gallium FIB, the slice thickness can be as low as 5 nm (Holzer and Cantoni, 2012). To minimize the radiation damage from the electron beam, a low beam voltage is preferable. However, a low beam voltage can lead to poor-quality compositional analysis due to the low yield of backscattering electrons. Since the cut face in serial sectioning is a flat block face and secondary electrons (SE) are sensitive to topography, the SE image would not provide as much information as the image formed by the backscattered electrons. A balance between signal yield and radiation damage needs to be explored. Despite carbon contamination and radiation damage, the extent of the radiolysis damage of a 2 kV beam is closely matched to the typical slice thickness, of 100 nm, and thus the electron beam damage from the imaging will be milled away in preparing the next slice, leaving little damage for further imaging. The 5 kV beam did not cause much damage to the thin film in this study due to a greater penetration than the film thickness, but that means subsequent layers will be partially damaged from SEM imaging of the previous 2–3 slices. Essentially, we are depositing damage deeper into the sample. The accumulated damage may finally lead to more severe damage in soft materials. Therefore, a beam voltage of 2 kV may be a good choice for imaging during FIB/SEM slice-and-view 3D tomography, despite causing the highest radiation damage.

5. Summary

Irradiation damage by low voltage electron beams to EMbed 812 epoxy resin in a scanning electron microscope was studied using scanning transmission X-ray microscopy. We found that the carbon contamination is the dynamic result of electron induced carbon deposition and mass loss process and depends on the beam voltage and exposure time. In our study, a 2 kV electron beam energy led to the most severe carbon contamination of the resin thin film sample due to (i) close match of electron range and sample thickness, (ii) a more significant deposition process than mass loss process, and (iii) more radiolysis damage than a 1 keV or 5 keV beam energy. The decrease of the 288.3 eV peak height and increase of the 286 eV peak height can be attributed to $C = O$ bond breaking. Radiolysis damage of resin thin films depends not only on dose but also whether or not the inelastic scattering is confined within the sample. We found that, for a 100 nm polymer film, radiolysis damage caused by 2 kV electrons is more severe than that from 1 kV or 5 kV electrons. To achieve a balance between imaging quality and extent of electron beam damage, 2 kV is a good choice for SEM imaging in FIB/SEM 3D tomography applications to soft matter samples, when the slice thickness is ˜100 nm.

Acknowledgements

The research work was supported by funding from the Natural Sciences and Engineering Research Council of Canada and the Ontario Centres of Excellence. We thank all the staff scientists from various facilities and institutes, including Marcia Reid (FHS, McMaster University), the Canadian Centre for Electron Microscopy (CCEM) and the Canadian Light Source (CLS). Research described in this paper was performed at the CCEM and CLS, which are supported by the Canadian Foundation for Innovation.

Appendix A. Supplementary data

Supplementary material related to this article can be found, in the online version, at doi:https://doi.org/10.1016/j.micron.2019.02.003.

References

Bassim, N.D., De Gregorio, B.T., Kilcoyne, A.L.D., Scott, K., Chou, T., Wirick, S., Cody, G., Stroud, R.M., 2012. Minimizing damage during FIB sample preparation of soft materials. J. Microsc. 245, 288–301.
Bassim, N., Scott, K., Giannuzzi, L.A., 2014. Recent advances in focused ion beam technology and applications. MRS Bull. 39, 317–325.
Burnett, T.L., Kelley, R., Winiarski, B., Contreras, L., Daly, M., Gholinia, A., Burke, M.G., Withers, P.J., 2016. Large volume serial section tomography by Xe Plasma FIB dual beam microscopy. Ultramicroscopy 161, 119–129.
Drouin, A.R.C.D., 2011. CASINO v2.5.0.CASINO v2.5.0.
Du, M., Jacobsen, C., 2018. Relative merits and limiting factors for x-ray and electron microscopy of thick, hydrated organic materials. Ultramicroscopy 184, 293–309.
Egerton, R.F., Li, P., Malac, M., 2004. Radiation damage in the TEM and SEM. Micron 35, 399–409.
Egerton, R.F., Wang, F., Crozier, P.A., 2006. Beam-induced damage to thin specimens in an intense electron probe. Microsc. Microanal. 12, 65–71.
Egerton, R.F., Lazar, S., Libera, M., 2012. Delocalized radiation damage in polymers. Micron 43, 2–7.
Giannuzzi, L.A., Stevie, F.A., 1999. A review of focused ion beam milling techniques for TEM specimen preparation. Micron 30, 197–204.
Holzer, L., Cantoni, M., 2012. Review of FIB-tomography. Nanofabrication Using Focused Ion and Electron Beams: Principles and Applications 559201222. pp. 410–435.
Jacobsen, C., Wirick, S., Flynn, G., Zimba, C., 2000. Soft X-ray spectroscopy from image sequences with sub-100 nm spatial resolution. J. Microsc.-Oxf. 197, 173–184.
Jiang, N., Spence, J.C.H., 2012. On the dose-rate threshold of beam damage in TEM. Ultramicroscopy 113, 77–82.
Joy, D.C., Joy, C.S., 1995. Dynamic charging in the low voltage SEM. Microsc. Microanal. 1, 109–112.
Joy, D.C., Joy, C.S., 1998. Study of the dependence of E2 energies on sample chemistry. Microsc. Microanal. 4, 475–480.
Koval, Y., Borzenko, T., Dubonos, S., 2003. Use of polymethylmethacrylate for pattern transfer by ion beam etching: improvement of etching homogeneity and patterning quality. J. Vac. Sci. Technol. B 21, 2217–2219.
Lehnert, T., Lehtinen, O., Algara-Siller, G., Kaiser, U., 2017. Electron radiation damage mechanisms in 2D MoSe2. Appl. Phys. Lett. 110, 4.
Leontowich, A.F.G., Hitchcock, A.P., 2012. Secondary electron deposition mechanism of carbon contamination. J. Vac. Sci. Technol. B 30.
Leontowich, A.F.G., Hitchcock, A.P., Tyliszczak, T., Weigand, M., Wang, J., Karunakaran, C., 2012. Accurate dosimetry in scanning transmission X-ray microscopes via the cross-linking threshold dose of poly(methyl methacrylate). J. Synchrot. Radiat. 19, 976–987.
Li, X., Sun, M., Shan, C., Chen, Q., Wei, X., 2018a. Mechanical properties of 2D materials studied by in situ microscopy techniques. Adv. Mater. Interfaces 5, 1701246.
Li, X., Sun, M., Wei, X., Shan, C., Chen, Q., 2018b. 1D piezoelectric material based nanogenerators: methods, materials and property optimization. Nanomaterials 8, 188.
Longieras, N., Sebban, M., Palmas, P., Rivaton, A., Gardette, J.L., 2007. Degradation of epoxy resins under high energy electron beam irradiation: radio-oxidation. Polym. Degrad. Stabil. 92, 2190–2197.
Rothmann, M.U., Li, W., Zhu, Y., Liu, A., Ku, Z.L., Bach, U., Etheridge, J., Cheng, Y.B., 2018. Structural and chemical changes to CH3NH3PbI3 induced by electron and gallium ion beams. Adv. Mater. 30, 7.
Scott, K., 2011. 3D elemental and structural analysis of biological specimens using electrons and ions. J. Microsc. 242, 86–93.
Stöhr, J., 2013. Springer science & business media. NEXAFS Spectroscopy.
Tapia, J.C., Kasthuri, N., Hayworth, K.J., Schalek, R., Lichtman, J.W., Smith, S.J., Buchanan, J., 2012. High-contrast en bloc staining of neuronal tissue for field emission scanning electron microscopy. Nat. Protoc. 7, 193–206.
Urquhart, S.G., Ade, H., 2002. Trends in the carbonyl core (C 1s, O 1s) -& pi*c=o transition in the near-edge X-ray absorption fine structure spectra of organic molecules. J. Phys. Chem. B 106, 8531–8538.
Wang, J., Button, G.A., West, M.M., Hitchcock, A.P., 2009a. Quantitative evaluation of radiation damage to polyethylene terephthalate by Soft x-rays and high-energy electrons. J. Phys. Chem. B 113, 1869–1876.
Wang, J., Morin, C., Li, L., Hitchcock, A.P., Scholl, A., Doran, A., 2009b. Radiation damage in soft X-ray microscopy. J. Electron Spectrosc. Relat. Phenom. 170, 25–36.
Xu, Y.M., Shi, L.A., Zhang, X.T., Wong, K.W., Li, Q., 2011. The electron beam irradiation damage on nanomaterials synthesized by hydrothermal and thermal evaporation methods-An example of ZnS nanostructures. Micron 42, 290–298.